Met. Mater. Int., Vol. 20, No. 4 (2014), pp. 629~639
doi: 10.1007/s12540-014-4007-0

Electrochemical Characteristics and Interfacial Contact Resistance of Multi-Layered Ti/TiN Coating for Metallic Bipolar-Plate of Polymer Electrolyte Membrane Fuel Cells

Jae-Bong Lee* and In Hwan Oh

Kookmin University, School of Advanced Materials Engineering, 861-1 Jeongneung-dong, Seongbuk-gu, Seoul 136-702, Korea

(received date: 12 August 2013 / accepted date: 1 December 2013)

Metallic bipolar-plates have advantages over non-porous graphite ones due to their higher mechanical strength and better electrical conductivity. However, corrosion resistance and interfacial contact resistance are major concerns that remain to be solved, since metals such as stainless steels may develop oxide layers that decrease electrical conductivity, thus lowering fuel cell efficiency. In this study, multi-layered nitride coatings consisting of Ti and TiN were deposited on 316L stainless steel (SS316L) by a D.C magnetron sputtering method to enhance the corrosion resistance and to lower the interfacial contact resistance (ICR) of metallic bipolar-plates for a polymer electrolyte membrane fuel cell (PEMFC). Electrochemical methods were conducted and ICRs of the coated specimens were measured to investigate the potential of the coated metallic bipolar-plate for use in PEMFCs. The multi-layered Ti/TiN coating deposited on SS316 showed lower ICR values than the single-layered TiN coating, and improved corrosion resistance when the PEMFC was not in operation while the degradation of the coating layer was observed in both cathodic and anodic working environments.

Keywords: bipolar plate, metal, nitride, PEMFC, passive film, coating, corrosion

1. INTRODUCTION

In a polymer electrolyte membrane fuel cell (PEMFC) stack, a bipolar-plate is a key element as it accounts for 80% of the total weight and over 50% of the total cost of the stack. More recent reports show that the relative cost has fallen to about 25% of the stack, yet this remains a very significant amount. In order to realize the economic feasibility of PEMFCs, there is a need to lower the cost of the bipolar-plates. Since the fabrication of traditional non-porous graphite is so difficult and expensive due to its brittleness, it's necessary to develop alternatives which have reasonable costs and suitable properties for PEMFCs [1].

The bipolar plates in the stacks play vital functions, such as carrying electric current away from each cell, distributing fuel and oxidant homogeneously within individual cells, separating individual cells, and facilitating the water management within the cell [2]. A variety of materials have been proposed for the manufacturing of bipolar plates capable of performing these multiple functions. The main properties that the materials must have for application in a bipolar plate are well established by the United States Department of Energy (DOE), as shown in Table 1 [3].

Metallic bipolar plates such as stainless steels are attractive candidates due to their high resistance to mechanical shocks and vibrations that could lead to cracking and leaking of reactant gases, their good electrical conductivity, and easy manufacturability at low cost [4]. However, it is generally agreed that stainless steels are prone to chemical attack in the acidic and humid environments of PEMFCs. Stainless steels operating in a fuel cell with a pH of 2-4 and temperature around 70 °C may suffer from dissolution. Their corrosion products may poison the catalysts in the polymeric membrane, and the oxide layer formed on the metal surface increases the ICR, decreasing the power output of the fuel cell [5].

The use of corrosion resistant and high conductive coatings on the metal is one of the widely studied surface modification techniques for overcoming the problems that metallic bipolar plates may have. Nitrides, such as TiN, CrN, and AlN, may be attractive candidates as coating materials for bipolar plates because of their excellent corrosion resistance and metal-like electrical conductivity. Li *et al*. [6] reported that a TiN coating deposited by physical vapor deposition (PVD) on 316L stainless steel (SS316L) resulted in an improvement in the corrosion resistance. Cho *et al*. [7] also found that a TiN coating on a SS316L substrate provided good electrochemical performance in the fuel cell environment.

*Corresponding author: leejb@kookmin.ac.kr

Table 1. Required chemical and physical properties for bipolar plates of PEMFCs. [3]

Properties	Required values
H_2 gas permeability	$< 2 \times 10^{-6} cm^3 cm^{-2} \cdot sec$ in 60~90 °C, 3 atm, (<0.1 mAc m^{-2})
Corrosion resistance	< 1 $mAcm^{-2}$ (0.1 V, H_2 anode) (0.6 V, Air cathode) in 60~90 °C, pH3, 1 mM~1 M H_2SO_4/2 ppm F^- solution
Interfacial contact resistance	< 10 $m\Omega \cdot cm^2$ in 100~150 Ncm^{-2}
Cost	<10 US$$kW^{-1}$ (500,000 stack/year)

However, it is well known that PVD coatings are usually embedded with defects, such as pin-holes. As a result, the protection of the substrate can fail, leading to a strong local corrosion attack. As illustrated by many reports [8-10], such corrosion attacks on coated materials can be reduced by the deposition of multi-layered coatings. The improvement in corrosion resistance produce by multi-layered coatings is due to the reduced number of defects, which can be fully blocked by corrosion products or by a lack of straight diffusion channels through the coatings.

This study focused on multi-layered Ti/TiN coated on SS316L by a D.C magnetron sputtering method as alternative materials for the replacement of graphite. The corrosion behaviors of the multi-layered Ti/TiN coating were investigated in simulated anodic and cathodic environments for PEMFCs by using electrochemical measurement techniques. The ICR between the coatings and gas diffusion layer (GDL) was also measured.

2. EXPERIMENTAL PROCEDURES

A D.C. magnetron sputtering method was used for the deposition of the coatings on SS316L. The chemical composition of SS316L is shown in Table 2. The SS316L substrates were discs 16 mm in diameter and 3 mm in thickness. Prior to deposition, they were wet-ground with 320, 600, 800, 1200 grit SiC abrasive paper, polished with a suspension of 1 μm alumina powder, cleaned with acetone and distilled water in an ultrasonic cleaner after immersion in 7% H_2SO_4 for 10 sec for surface activation, and then finally dried with N_2 gas.

Before the multi-layered coating was applied, single-layered TiN coatings were deposited on the SS316L under a N_2 flow, to determine the optimized deposition conditions. A gas mixture of N_2 (99.99%) and Ar (99.99%) was used for the deposition and the N_2 flow rate was varied between the values of 4, 10, 15, 20, and 25 sccm (Standard Cubic Centimeter per Minute, $cm^3 min^{-1}$) with a fixed working pressure

Table 3. Deposition conditions for Ti and TiN coating layers

		TiN(outer)	Ti(inner)
Target		Ti(99.99%)	Ti(99.99%)
Pressure (torr)	Base pressure (torr)	1×10^{-6}	1×10^{-6}
	Working pressure (torr)	3.5×10^{-3}	3×10^{-3}
Gas flow rate (sccm)	N_2 (sccm)	4, 10, 15, 20, 25	0
	Ar (sccm)	0, 5, 10, 15, 20	20
Deposition temperature (°C)		32	32
Thickness of coatings (nm)		140	120

(3.5×10^{-3} torr) in the chamber. In order to investigate any effect of the N_2 flow rate on the TiN coating properties, potentiodynamic polarization and potentiostatic polarization tests were conducted in simulated PEMFC environments and the ICR of each single-layered TiN coating was measured.

After determining the optimized TiN deposition conditions, a multi-layered Ti/TiN coating was deposited on SS316L. First, a Ti coating layer was deposited on SS316L and an optimized TiN coating layer was deposited on the Ti coating layer. More details of each deposition condition are shown in Table 3.

The surface morphology of the coatings with single or multi-layered structure and the thickness of multi-layered coatings were examined by field emission scanning electron microscope (FE-SEM). The N/Ti ratio of the TiN coatings as a function of N_2 flow rate was also measured by an energy dispersive spectroscopy (EDS) analysis attachment for a FE-SEM.

ICR values for both coated and uncoated specimens and gas diffusion layers (GDL, SGL 10 series BA) were measured with respect to the change of compaction force. The ICR measurement method used by Wang et al. [11-16] was modified by decreasing the number of interfaces for more accurate and simpler measurement, as shown in Fig. 1. With this method, the measured resistance (R_{total}) is twice the resistance between the GDL and coatings ($R_{GDL/coating}$), which can

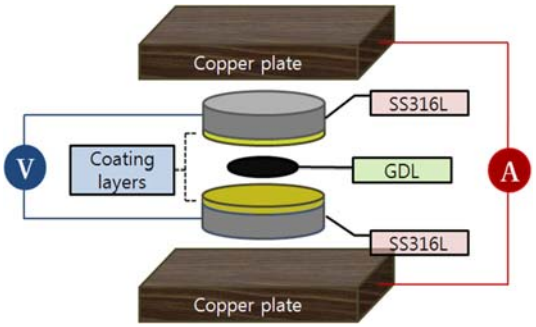

Fig. 1. Schematic setup for the measurement of interfacial contact resistance.

Table 2. Chemical composition of SS316L (wt%)

C	Mn	P	S	Si	Cr	Ni	Co	Cu	Mo	N	Sn	Nb
0.014	1.70	0.028	0.001	0.35	16.30	10.13	0.26	0.43	2.09	0.04	0.009	0.014

be expressed as $R_{total}=2R_{GDL/coating}$. The range of compaction force was from 20 Ncm^{-2} to 220 Ncm^{-2}.

Changes of ICR values at a compaction force of 140 Ncm^{-2} were also investigated for various immersion times (0, 2, 24, 48, 72 h) in the PEMFC working environments. 1 M H_2SO_4/ 2 ppm F^- solution at 70 °C with H_2 or air purging was chosen for immersion to simulate the anodic and cathodic environments, respectively. The applied potential was 0.1 V_{SCE} (anode) or 0.6 V_{SCE} (cathode) with respect to the saturated calomel electrode (SCE) during the immersion, depending on the test.

Three kinds of electrochemical tests (potentiodynamic polarization, potentiostatic polarization, and electrochemical impedance spectroscopy (EIS) were conducted in order to investigate the corrosion behaviors of the specimens. All tests were conducted in a three-electrode system test unit with a platinum counter electrode and a Ag/AgCl, 3M KCl electrode as the reference electrode, but the Ag/AgCl electrode unit was converted to a saturated calomel electrode (SCE) unit in all results of the tests. The exposed coating area was 1 cm^2.

In the potentiodynamic polarization test, the initial potential was -0.2 V vs. open circuit potential (OCP), and the final potential was 1.2 V_{SCE}. The scan rate was 0.5 mVs^{-1}. The specimens were stabilized at the OCP for 600 sec. The current density change under the operating potential in the simulated PEMFC environments was monitored by the potentiostatic polarization test for 72 h. The applied potential was -0.1 V_{SCE} with H_2 purging (anode) and 0.6 V_{SCE} with air purging (cathode). After the test, the inductively coupled plasma (ICP) analysis was conducted by collecting part of the solution to analyze the concentration of metal ions dissolved from the specimen.

In order to measure the change of polarization resistance with immersion time (0, 2, 24, 48, 72 h) in the simulated PEMFC working environments, an EIS test was conducted after each immersion. In the immersion conditions, the applied potential was -0.1 V_{SCE} with H_2 purging (anode) or 0.6 V_{SCE} with air purging (cathode). An alternating current signal with the frequency range of 10^5 to 10^{-2} Hz and an amplitude of 10 mV (rms) was applied to the multi-layered Ti/TiN coating at the corrosion potential to obtain polarization resistances.

3. RESULTS

3.1. Determination of the optimized deposition condition for TiN coating

The TiN coating was deposited on SS316L by a D.C magnetron sputtering method as a function of the N_2 flow rate (4, 10, 15, 20, 25 sccm). Total deposition time was 25 min and the thickness of the TiN coating was 140 nm. Figure 2(a) shows a FE-SEM micrograph of the surface of the TiN coating (N_2 flow rate: 20 sccm). All TiN coatings exhibited similar surface morphologies, and some defects, such as pin-holes and

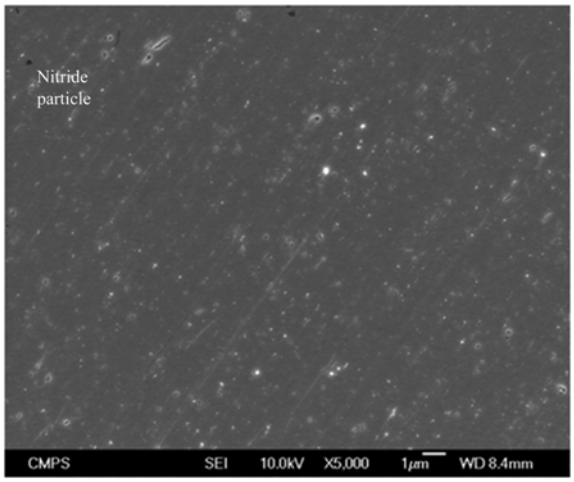

(a)

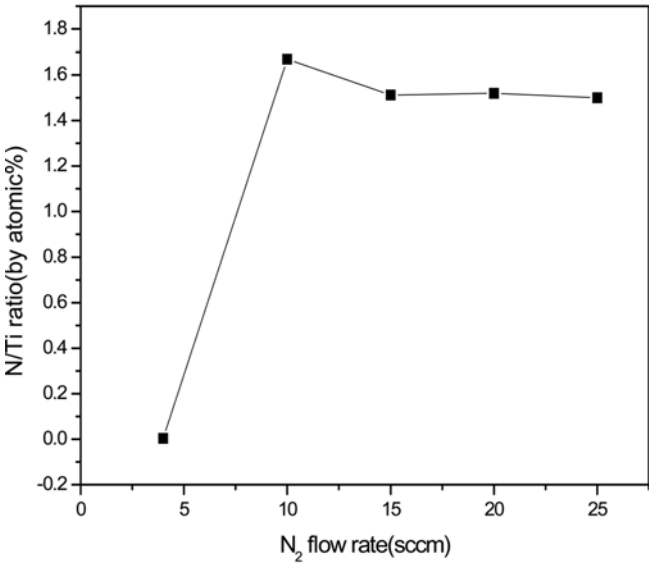

(b)

Fig. 2. (a) FE-SEM micrographs for the TiN coating (N_2 flow rate : 20 sccm) on SS316L and (b) N/Ti ratio of TiN coatings on SS316L as a function of N_2 flow rate.

particles, were observed on their surfaces. The particles were mainly nitrides, as analyzed by EDS. From Fig. 2(b), where the N/Ti ratio of the TiN coating as a function of N_2 flow rate was plotted, it is shown that the N/Ti ratio was almost 0 at a N_2 flow rate of 4 sccm, meaning that the coating was pure Ti rather than TiN. The values of the N/Ti ratio became saturated at about 1.6 when the N_2 flow rate was over 10 sccm.

The ICRs of the SS316L and TiN coatings deposited with various N_2 flow rates were measured as a function of compaction force (Fig. 3). ICR values of all the TiN coatings gradually decreased as the compaction force increased due to an increase in the contact area between the coating and GDL. The TiN coatings exhibited much lower ICR values than uncoated SS316L did. The reason for this is that TiN has

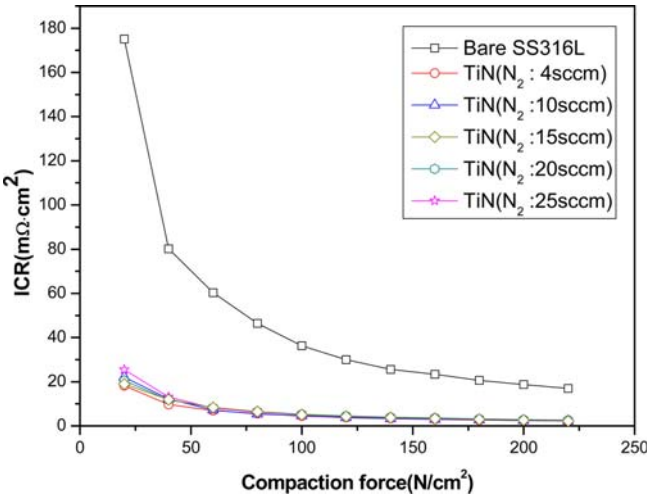

Fig. 3. ICR of SS316L and TiN coatings (N_2 flow rate : 4, 10, 15, 20, 25 sccm) as a function of compaction force.

very good electrical conductivity and a passive film which formed on the surface of the SS316L increased the ICR. It is well known that passive films on stainless steel improve corrosion resistance, but also cause increases in electrical resistance between bipolar-plates and GDLs. ICR values of the TiN coatings were not influenced by the variation of the N_2 flow rate and all TiN coatings satisfied the ICR requirements for a DOE target (<10 mΩ·cm^2), while that of uncoated SS316L did not.

The potentiodynamic polarization curves for uncoated SS316L and TiN coatings in simulated PEMFC cathodic and anodic environments are shown in Fig. 4. Open circuit potentials of the TiN coatings were higher than those of uncoated SS316L in both cathodic and anodic environments, and also the TiN coatings had about 100-1000 times lower current densities than the SS316L did, except for the TiN coating prepared under a 4 sccm N_2 flow rate. This result indicated that the TiN coatings significantly improved corrosion resistance when the fuel cell was not in operation. However, the current densities of the TiN coatings increased with increases in the applied potential, but rapidly decreased at values higher than 0.6 V_{SCE} in both cathodic and anodic environments.

The TiN coatings exhibited similar passive behavior as uncoated SS316L above 0.6 V_{SCE}. This passive behavior was associated with the fact that the SS316L substrate was exposed to the electrolyte due to the dissolution of the TiN coating layer. In the case of the TiN coating deposited under a 4 sccm N_2 flow rate, the passive behavior was not observed because the composition of the coating was overwhelmed with Ti. The dissolution of the TiN coating layer resulted in a higher current density than that of uncoated SS316L at the PEMFC cathodic working potential (0.6 V_{SCE}), while the current densities of the TiN coatings at the PEMFC anodic working potential (-0.1 V_{SCE}) were still very low.

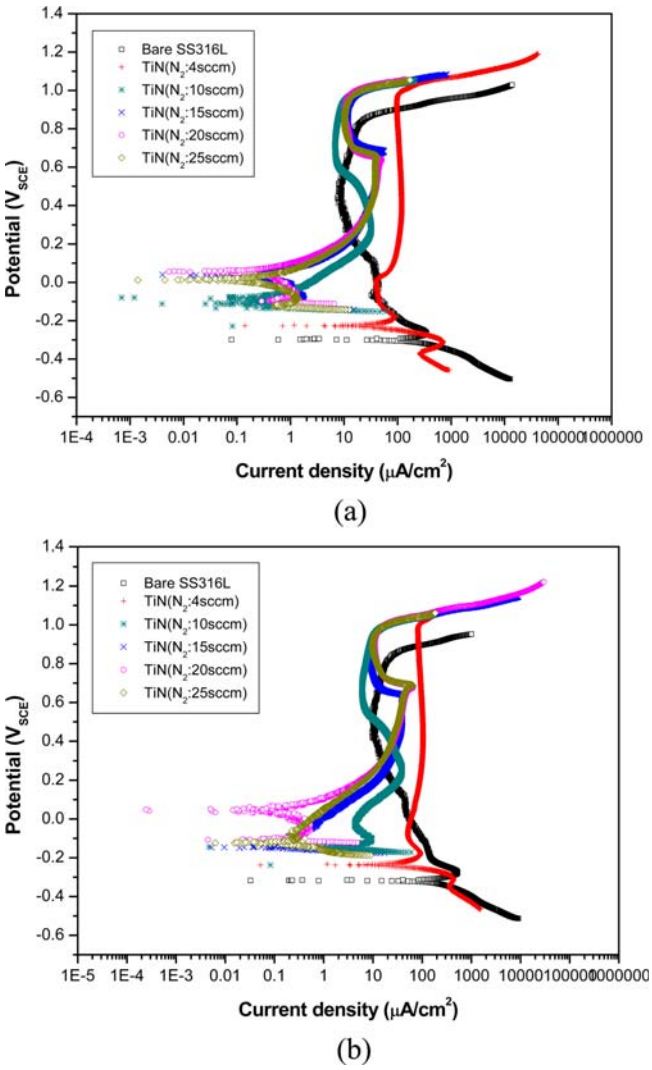

Fig. 4. Potentiodynamic polarization curves of SS316L and TiN coatings (N_2 flow rate : 4, 10, 15, 20, 25 sccm) in simulated PEMFC environments; (a) cathodic environment under air condition and (b) anodic environment at under H_2 condition.

Notably, for the TiN coating deposited with a 20 sccm N_2 flow rate, open circuit potentials were higher than the anodic working potential (-0.1 V_{SCE}) in the anodic environment at which current densities were negative. The potentiostatic polarization curves for the TiN coatings in the simulated PEMFC cathodic and anodic working environments are shown in Fig. 5, providing more information on the corrosion behavior of the TiN coatings. In the case of the cathodic working environment, the current densities of the TiN coatings increased, exhibiting very high values at the early stage of the test due to the dissolution of the TiN coatings.

However, as soon as the substrate was exposed to the electrolyte, the current densities decreased rapidly and became stable due to the passive film formed on the SS316L substrate, at the cathodic working potential (0.6 V_{SCE}). It was

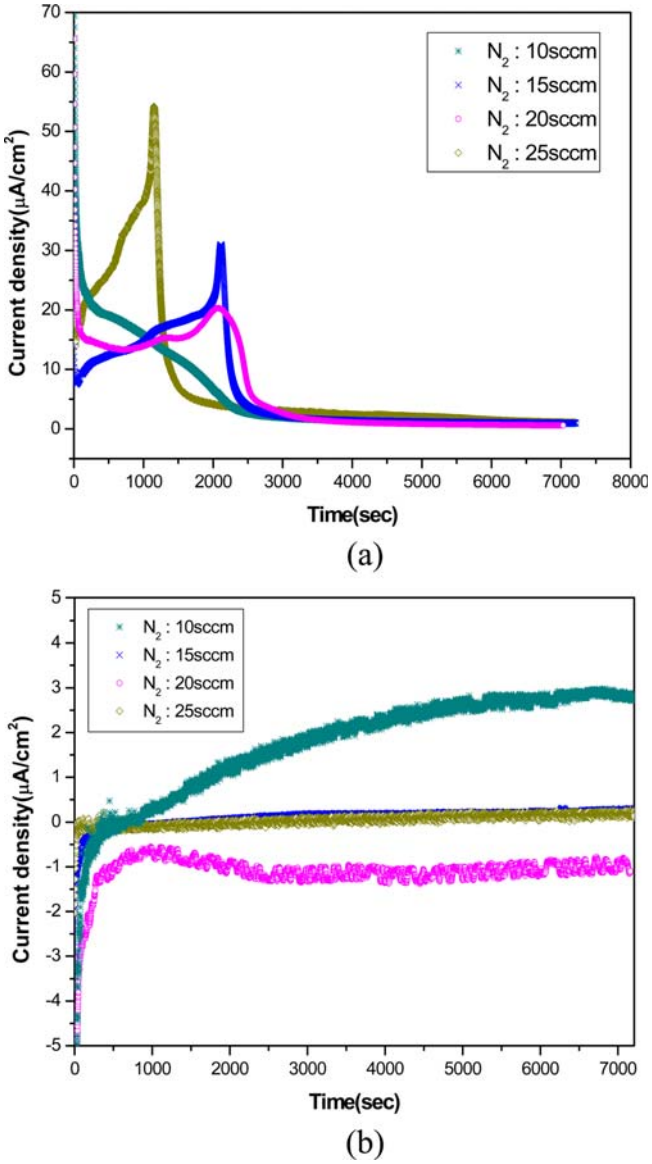

Fig. 5. Potentiostatic polarization curves of TiN coatings (N_2 flow rate: 10, 15, 20, 25 sccm) as a function of N_2 flow rate in simulated PEMFC working environments for 2 h; (a) cathodic working environment at 0.6 V_{SCE} under air condition and (b) anodic working environment at -0.1 V_{SCE} under H_2 condition.

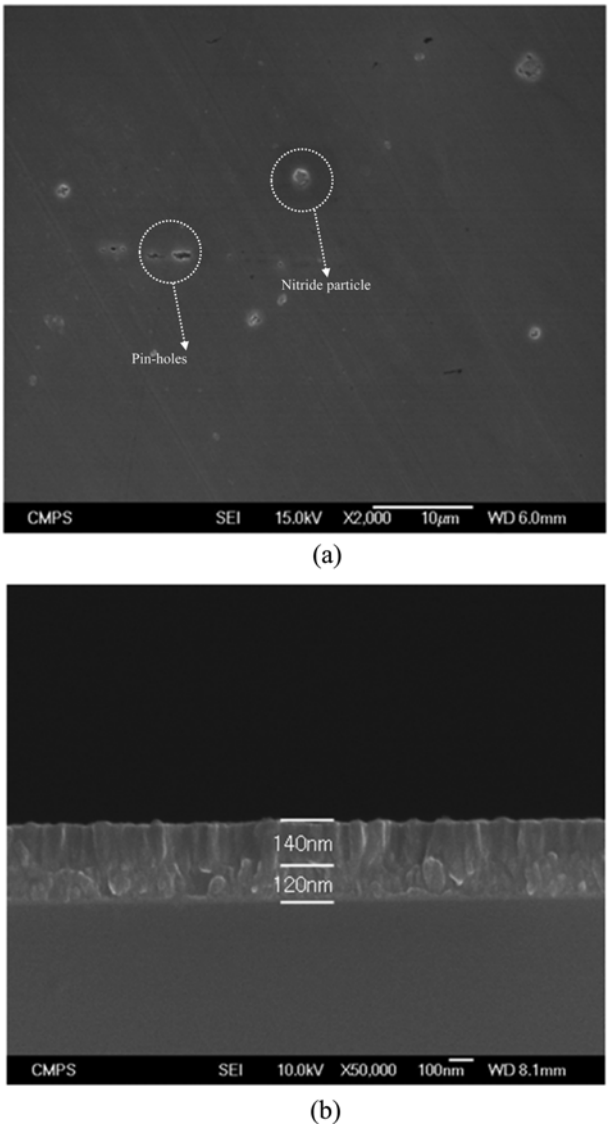

Fig. 6. FE-SEM micrographs for (a) the surface of the multi-layered Ti/TiN coating on SS316L and (b) a cross section of the multi-layered Ti/TiN coating on the Si substrate.

found that the dissolution rate of the TiN coatings increased in the order of 20 sccm < 15 sccm < 25 sccm < 10 sccm. However, in the case of the anodic working environment, the dissolution of the TiN coatings was not observed and all specimens exhibited very low current densities. Notably, the TiN coating deposited under a 20 sccm N_2 flow rate exhibited negative current densities.

3.2. FE-SEM micrographs of multi-layered Ti/TiN coating

From the results on measurements of ICR and corrosion resistance for TiN coatings as a function of N_2 flow rate, it was found that the TiN coating deposited at a 20 sccm N_2 flow rate exhibited excellent properties. Therefore, a TiN coating prepared with a 20 sccm N_2 flow rate was deposited on a Ti layer deposited on SS316L. The surface morphology and the cross section of the multi-layered Ti/TiN coating were observed by FE-SEM (Fig. 6). Compared with the single-layered TiN coating (Fig. 2), the multi-layered Ti/TiN coating had a significantly smaller quantity of particles and pin-holes on its surface. The total thickness of the multi-layered Ti/TiN coating was about 260 nm (Ti layer : 120 nm, TiN layer : 140 nm).

3.3. ICR measurement of multi-layered Ti/TiN coating

Figure 7 shows ICR values of the uncoated SS316L, sin-

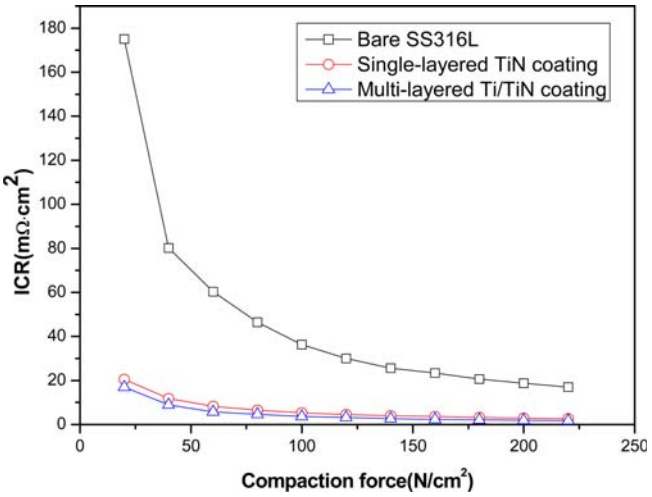

Fig. 7. ICRs of SS316L, single-layered TiN (N_2 flow rate : 20 sccm) and multi-layered Ti/TiN coatings as a function of compaction force.

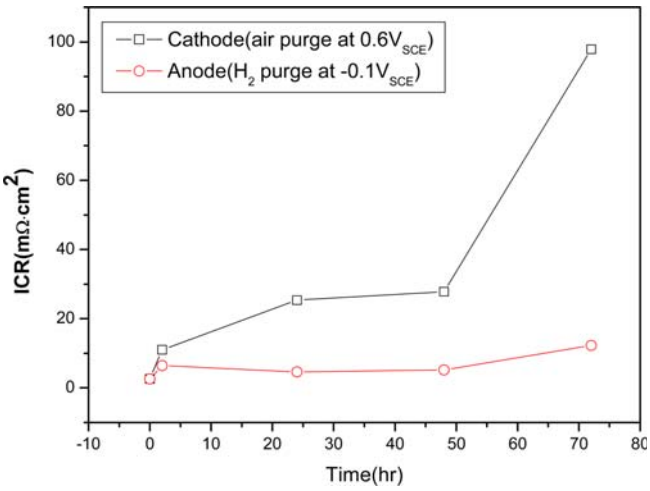

Fig. 8. Change of ICR of the multi-layered Ti/TiN coating at 140 Ncm^{-2} after various immersion times (0, 2, 24, 48, 72 h) in PEMFC cathodic and anodic environments.

gle-layered TiN (20 sccm) and multi-layered Ti/TiN coatings as a function of compaction force. ICRs of the multi-layered Ti/TiN coating gradually decreased as the compaction force increased, showing that they were slightly lower than those of the single-layered TiN coating.

The ICR values of all specimens with various compaction forces, i.e., the force at which bipolar-plates are pressed in the PEMFC stack, are shown in Table 4. Both the single-layered TiN and the multi-layered Ti/TiN coatings satisfied the ICR values for the DOE target at a compaction force of 140 Ncm^{-2}. ICR values of uncoated SS316L, single-layered TiN, and multi-layered Ti/TiN coatings were 25.6 $m\Omega \cdot cm^2$, 3.98 $m\Omega \cdot cm^2$, and 2.6 $m\Omega \cdot cm^2$, respectively.

Figure 8 shows the ICR values of the multi-layered Ti/TiN coating measured with a compaction force of 140 Ncm^{-2} for various immersion times (0, 2, 24, 48, 72 h) in the PEMFC working environments. In the cathodic working environment, an increase of the ICR of the multi-layered Ti/TiN coating was observed as the immersion time increased; also, all ICR values after immersion failed to satisfy the DOE requirements. This may be because the exposed Ti coating layer or the SS316L after the dissolution of the TiN coating layer was oxidized, thus forming oxides or hydroxides in the cathodic working environment.

On the other hand, the multi-layered Ti/TiN coating in the anodic working environment still exhibited low and stable ICR values and satisfied the DOE requirements for the whole range of immersion times. However, degradation of the coating layers was also observed after immersion in the anodic working environment, indicating that the substrate, SS316L, was widely exposed to the electrolyte. This may be attributed to a loss of adhesion between the Ti/TiN coating layers and the substrate due to corrosion products formed through defects in the coatings. This may be due to the unstable passive film formed on the SS316L substrate at the anodic working potential. Therefore, the ICR behavior of the multi-layered Ti/TiN coating in the anodic working environment followed that of an SS316L sample which had formed an unstable passive film on its exposed area, rather than that of the Ti/TiN coating layers.

In our previous study [17], the ICR of SS316L significantly increased after immersion in the PEMFC cathodic working environment, but decreased in the PEMFC anodic working environment. This behavior was due to the stability of the passive film on SS316L in the simulated PEMFC working environments. The unstable passive film which resulted in the corrosion of SS316L was dissolved as the immersion time increased in the anodic working environment, decreasing the ICR values.

3.4. Electrochemical characteristics of multi-layered Ti/TiN coating

Figure 9 shows the potentiodynamic polarization curves for uncoated SS316L, single-layered TiN, and multi-layered

Table 4. ICR values of SS316L, single-layered TiN and multi-layered Ti/TiN coatings as a function of compaction force

Specimens	ICR($m\Omega \cdot cm^2$)										
	20Ncm^{-2}	40Ncm^{-2}	60Ncm^{-2}	80Ncm^{-2}	100Ncm^{-2}	120Ncm^{-2}	140Ncm^{-2}	160Ncm^{-2}	180Ncm^{-2}	200Ncm^{-2}	220Ncm^{-2}
SS316L	175.1	80.15	60.35	46.37	36.32	30.02	25.6	23.39	20.59	18.74	17.03
TiN	20.53	11.8	8.29	6.47	5.33	4.55	3.98	3.6	3.21	2.85	2.66
Ti/TiN	17.01	8.97	5.73	4.64	3.63	3.16	2.6	2.34	2.12	1.92	1.74

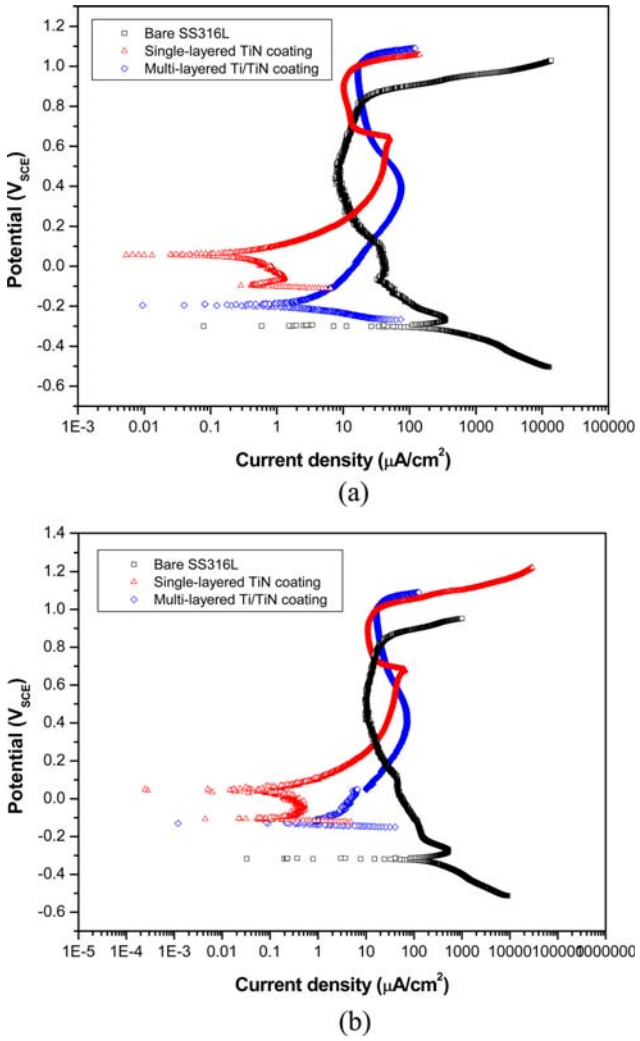

Fig. 9. Potentiodynamic polarization curves of SS316L, single-layered TiN, and multi-layered Ti/TiN coatings in simulated PEMFC environments; (a) cathodic environment under air condition and (b) anodic environment under H_2 condition.

Ti/TiN coatings in simulated PEMFC cathodic and anodic environments. Compared with the single-layered TiN coating, the multi-layered Ti/TiN coating exhibited a lower OCP and higher corrosion current density. Moreover, the multi-layered Ti/TiN coating had higher overall current densities with anodic polarization than the single-layered TiN coating. The dissolution of the TiN layer for the multi-layered Ti/TiN coating was observed to be more active and faster, representing different passive behaviors between single-layered TiN and multi-layered Ti/TiN coatings. This can be explained by the fact that for the multi-layered Ti/TiN coating, the Ti layer was exposed and passivated after the dissolution of the TiN layer, rather than the passivation of the SS316L substrate.

Figure 10 shows the potentiostatic polarization curves of the multi-layered Ti/TiN coating immersed in the simulated PEMFC cathodic and anodic working environments for 72 h.

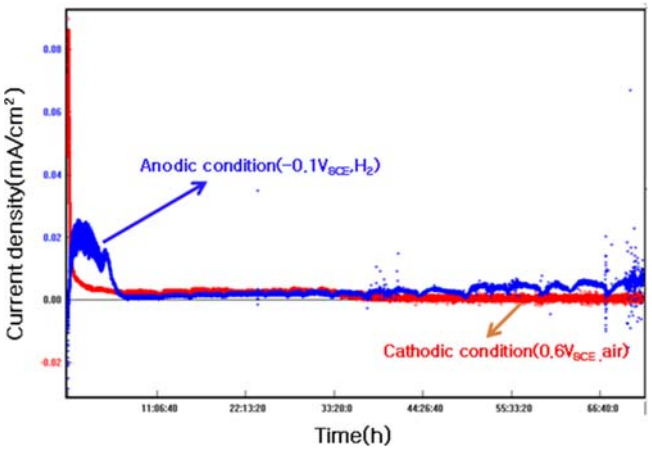

Fig. 10. Potentiostatic polarization curves of the multi-layered Ti/TiN coating in simulated PEMFC cathodic and anodic working environments for 72 h.

In the case of the cathodic working environment, the initial high values of the current densities reflected that the TiN layer was actively dissolved at the early stage of the test. After that, the Ti layer was exposed to the electrolyte and oxidized, resulting in a rapid decrease of the current density. Then, the current density became stable and low. An additional slight decrease of the current density was observed after about 33 h. This may be attributed to the passivation of widely exposed SS316L to the electrolyte. The penetration of the electrolyte into the substrate, SS316L, through pin-holes on the oxidized Ti layer may result in the passivation of SS316L and a loss of adhesion between SS316L and the oxidized Ti layer.

In the case of the anodic working environment, the multi-layered Ti/TiN coating exhibited a negative current density at the early stage of the test. After that, the current density increased for a moment and decreased rapidly with further increases in immersion time. Compared with the current density in the cathodic working environment, the current density was somewhat high and unstable in the anodic working environment during the latter half of the test. This potentiostatic polarization behavior of the multi-layered Ti/TiN coating can be explained by the degradation of the Ti/TiN coating layer and the unstable passive film on SS316L in the anodic working environment.

Since SS316L is not in a stable passive region, the area of the substrate exposed to the electrolyte through pin-holes in the Ti/TiN coating layer may corrode and cause corrosion products at the interface between the substrate and the Ti/TiN coating layer, which results in a loss of adhesion between the substrate and the Ti/TiN coating layer. As a result, degradation of the Ti/TiN coating layer may occur in the anodic working environment. Therefore, although there was no dissolution of the TiN coating layer in the anodic working environment, the Ti/TiN coating layer could be degraded.

Figure 11 shows the Nyquist plots of the multi-layered Ti/

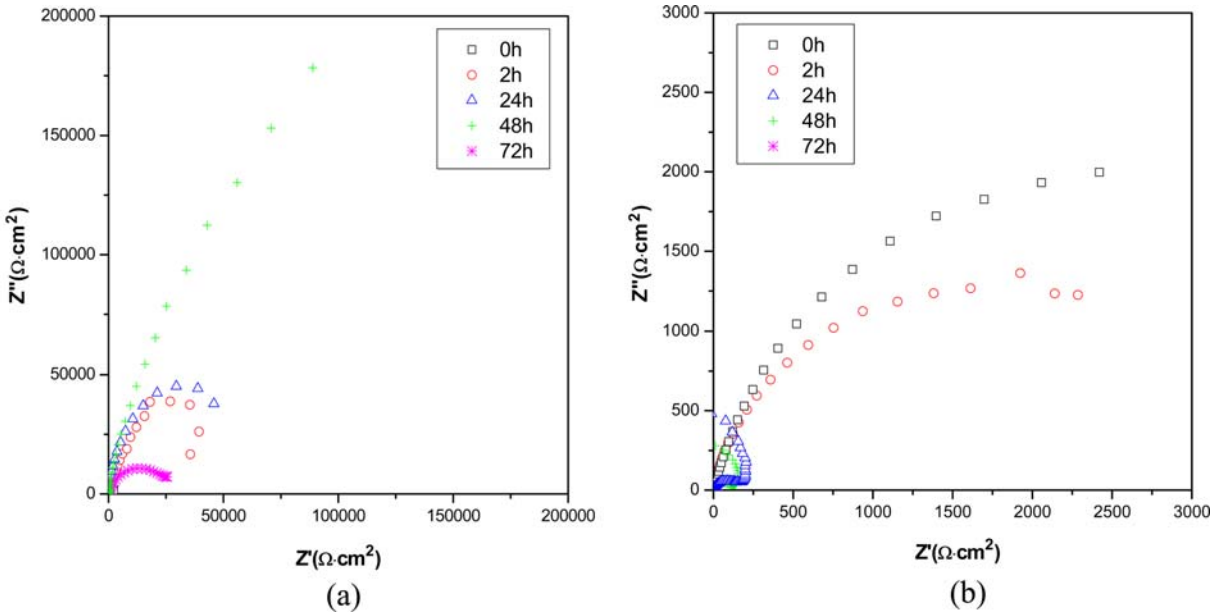

Fig. 11. Nyquist plots of multi-layered Ti/TiN coating for EIS data as a function of immersion time (0, 2, 24, 48, 72 r) in (a) cathodic working environment (0.6 V_{SCE}, air condition) and (b) anodic working environment (-0.1 V_{SCE}, H_2 condition).

TiN coating as a function of immersion time in the PEMFC working environments. In the cathodic working environment, the polarization resistance, which is represented by the diameters of the semicircles in the Nyquist plots, increased as the immersion time increased. This results from the passivation of the Ti layer and the substrate, SS316L, after being exposed to the electrolyte after the dissolution of the TiN coating layer. Similar semicircles observed for immersion times of 2 and 24 h were due to oxidation of the Ti coating layer after the dissolution of the TiN coating layer.

After an immersion time of 48 h, the polarization resistance increased dramatically due to the passivation of the substrate, SS316L, after the degradation of the oxidized Ti coating layer. The polarization resistance decreased again after an immersion time of 72 h. This is because the dissolution rate of the passive film on SS316L may be faster than that of the formation of the passive film. In the anodic working environment, the polarization resistance decreased as the immersion time increased. The polarization resistance for an immersion time of 2 h slightly decreased because the Ti/TiN coating layer still remained. However, after 24 h, the polarization resistance significantly decreased because the exposed substrate actively corroded after the degradation of the Ti/TiN coating layer.

All values of the polarization resistances for each immersion time were much lower than those in the cathodic working environment. This is because the substrate, SS316L corroded due to the formation of an unstable passive film in the anodic environment while it formed a stable passive film in the cathodic environment after the degradation of the Ti/TiN coating layer.

Figure 12 shows changes of the open circuit potentials (OCPs) of the multi-layered Ti/TiN coating after immersion in cathodic and anodic working environments. In the cathodic working environment, the OCP increased as the immersion time increased because the Ti coating layer and the substrate, SS316L, were exposed to the electrolyte and passivated after the dissolution of the TiN coating layer. In the anodic working environment, the OCP briefly increased after an immersion time of 2 h and then decreased with further increases in immersion time. But, compared with the change in the cathodic working environment, change was slight in the anodic working environment. These results were consistent with those of

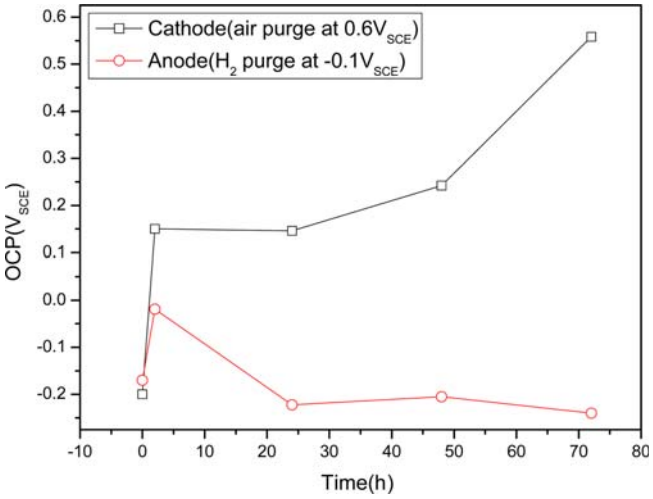

Fig. 12. Change of open circuit potentials (OCPs) of multi-layered Ti/TiN coating as a function of immersion time (0, 2, 24, 48, 72 h) in simulated PEMFC cathodic and anodic working environments.

Table 5. Metal ion concentration of the solution after 72 h potentiostatic polarization test in the simulated PEMFC cathodic and anodic working environments

Specimens		Dissolved metal ion concentration (ppm)				Total concentration of metal ion (ppm)
		Fe	Ti	Cr	Ni	
Ti/TiN	Cathode	0.03	0.27	0.02	0.015	0.335
	Anode	1.86	0.08	0.32	0.45	2.71

the potentiostatic tests.

3.5. ICP analysis for dissolved metal ions

A metallic bipolar-plate could corrode in the acidic and humid environments of PEMFCs. The dissolved metal ions due to corrosion may poison the membrane electrode assembly (MEA), decreasing the power output of a PEMFC [18]. Therefore, ICP analysis was conducted to investigate the concentration of dissolved metal ions in the test solution.

Table 5 shows the result of the ICP analysis for dissolved metal ion concentrations from the solution after a 72 h potentiostatic polarization test for the multi-layered Ti/TiN coating. The solution after the test in the cathodic working environment contained a large amount of Ti ions and small amounts of Fe, Cr, and Ni ions, which are metal elements dissolved from the substrate, SS316L. This is due to the dissolution of the TiN coating layer and the formation of a stable passive film on the substrate in the cathodic working environment; this is in good agreement with the electrochemical test results.

On the other hand, the solution after the test in the anodic working environment contained a small amount of Ti ions and large amounts of Fe, Cr, and Ni ions. This is because the TiN coating layer did not dissolve in the anodic working environment and only the degradation of the Ti/TiN coating occurred due to the loss of adhesion between the coating and the substrate. Moreover, the total concentration of metal ions in the anodic working environment was much larger than that in the cathodic working environment because the exposed substrate in the anodic environment, after the degradation of the Ti/TiN coating, was actively corroded due to the unstable passive film formed on the SS316L substrate.

4. DISCUSSION

4.1. ICR of multi-layered Ti/TiN coating

With respect to the result of the measurement of the ICR, the multi-layered Ti/TiN coating exhibited significantly improved electrical conductivity. Prior to deposition, removing the passive film on SS316L may improve the electrical conductivity, and TiN itself also has excellent conductivity. In addition to this, the Ti metal layer between the TiN and SS316L may lead to a low ICR value for the multi-layered Ti/TiN coating. However, the ICR values dramatically increased after immersion in the PEMFC cathodic working environment. This is attributed to the passivation of the Ti coating layer and the SS316L after the dissolution of the TiN coating layer in the cathodic working environment. On the other hand, the ICR values in the anodic working environment were slightly changed and low due to the unstable passive film on SS316L, in spite of the degradation of the Ti/TiN coating layer.

4.2. Interpretation on corrosion mechanisms of multi-layered Ti/TiN coating in PEMFC working environments

Based upon the results of the electrochemical tests and ICR measurement, it was found that there were several steps to the corrosion behavior of the multi-layered Ti/TiN coating in the PEMFC working environments. The schematic diagram of the corrosion mechanism for the multi-layered Ti/TiN coating in the PEMFC cathodic working environment is shown in Fig. 13.

The first step is the dissolution of the TiN coating layer at the cathodic working potential (0.6 V_{SCE}). The second step is the oxidation of the widely-exposed Ti coating layer and the passivation of local areas of the SS316L substrate, which are exposed to the electrolyte through defects (pin-holes) in the Ti coating layer. Finally, SS316L gradually forms a stable passive film on the locally-exposed areas at 0.6 V_{SCE}, which results in a loss of adhesion between the oxidized Ti coating layer and SS316L. Therefore, degradation of the oxidized Ti coating layer occurs and the stable passive film is formed on the entire surface of the SS316L.

The dissolution of the coating layer and the exposure and passivation of the substrate provide a multi-layered Ti/TiN coating with increased OCP and polarization resistance in the cathodic working environment, resulting in a large amount of dissolved Ti ions, which may contaminate the MEAs of PEMFCs. The contamination of MEAs decreases the efficiency of PEMFCs. Moreover, the formation of a stable passive film on the substrate increases the electrical resistivity

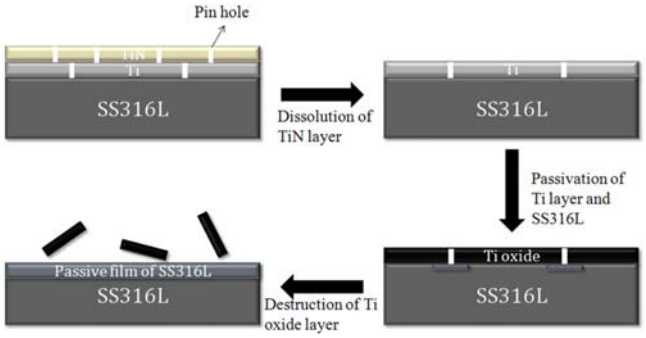

Fig. 13. Schematic diagram for corrosion behavior of multi-layered Ti/TiN coating in cathodic working environment.

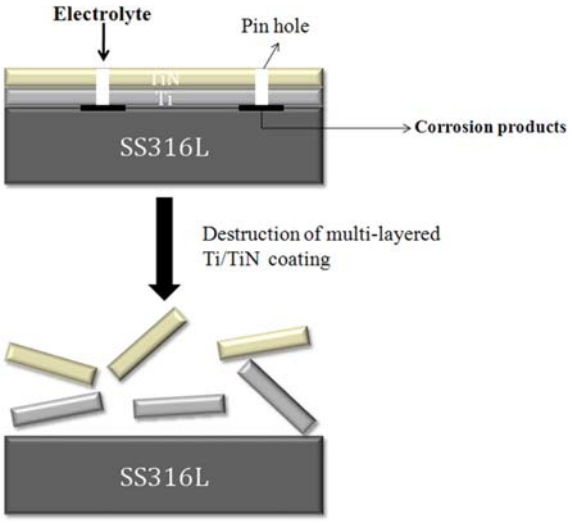

Fig. 14. Schematic diagram for corrosion behavior of multi-layered Ti/TiN coating in anodic working environment.

of the bipolar-plates. Consequently, the PEMFC efficiency is also negatively affected due to the increase of the ICR as the oxide layer grows.

Figure 14 shows the schematic diagram of the corrosion mechanism for the multi-layered Ti/TiN coating in the PEMFC anodic working environment. Although the TiN coating layer is not dissolved at the anodic working potential (-0.1 V_{SCE}), the SS316L substrate is corroded, after being locally exposed to the electrolyte through defects (pin-holes) on the Ti/TiN coating layer. This occurs because SS316L forms an unstable passive film at the anodic working potential.

Therefore, the first step of the corrosion mechanism for the multi-layered Ti/TiN coating in the anodic working environment is the production of corrosion products at the interface between SS316L and the coating layer, resulting in a loss of adhesion between SS316L and the coating layer. The second step is the degradation of the multi-layered Ti/TiN coating layer and the widely-exposed SS316L, which is actively corroded due to the unstable passive film on its surface. Therefore, the polarization resistance rapidly decreases as the immersion time in the anodic working environment increases. However, the change of the OCP and ICR of the multi-layered Ti/TiN coating as a function of immersion time in the anodic working environment is not significant. In addition, the corrosion of SS316L causes a large amount of metal ions, such as Fe, Cr, and Ni.

5. CONCLUSIONS

From the investigation of the electrochemical characteristics and ICR measurements of multi-layered Ti/TiN coatings deposited by D.C magnetron sputtering method on SS316L, the following conclusions were obtained.

(1) The multi-layered Ti/TiN coating deposited on SS316L with the optimized deposition conditions (20 sccm N_2 flow rate), showed lower ICR values than the single-layered TiN coating, and improved corrosion resistance in the simulated PEMFC environments when the PEMFC was not in operation. However, degradation of the coating layer was observed in both cathodic and anodic working environments.

(2) In the cathodic working environment, the dissolution of the TiN coating layer and the passivation of both the Ti coating layer and the substrate, SS316L were observed. This resulted in the loss of adhesion between the oxidized Ti coating layer and SS316L. The dissolution of the coating layer and the passivation of the substrate provide a multi-layered Ti/TiN coating with increased ICR, causing a large amount of dissolved Ti ions.

(3) In the anodic working environment, the substrate locally exposed to the electrolyte through defects on the coating layer corroded. The adhesion between the substrate and the coating layer was weakened due to the unstable passive film formed on the surface of SS316L at the anodic working potential. Therefore, although the ICR satisfied the DOE requirement after immersion, the corrosion resistance decreased with the increase in immersion time in the anodic working environment, causing a large amount of dissolved metal ions such as Fe, Cr and Ni.

ACKNOWLEGEMENT

This work was supported by the National Research Foundation of Korea Grant funded by the Korean Government (2009-0074278).

REFERENCES

1. H. Tawfik, Y. Hung, and D. Mahajan, *J. Power Sources* **163**, 755 (2006).
2. H. Tsuchiya and O. Kobayashi, *Int. J. Hydrogen Energ*. **29**, 985 (2004).
3. A. Hermann, T. Chaudhuri, and P. Spagnol, *Int. J. Hydrogen Energ*. **30**, 1297 (2005).
4. R. A. Antunes, M. C. L. Oliveira, G. Ett, and V. Ett, *Int. J. Hydrogen Energy* **35**, 3632 (2010).
5. A. Kraytsberg, M. Auinat, and Y. Ein-Eli, *J. Power Sources* **164**, 697 (2007).
6. M. Li, S. Luo, C. Zeng, J. Shen, H. Lin, and C. Cao, *Corros. Sci*. **46**, 1369 (2007).
7. E. A. Cho, U. S. Jeon, I. H. Oh, and S. G. Kang, *J. Power Sources* **142**, 177 (2005).
8. W. Y. Ho, H. J. Pan, C. L. Chang, D. Y. Wang, and J. J. Hwang, *Surf. Coat. Technol*. **202**, 1297 (2007).
9. S. Rudenja, C. Leygraf, J. Pan, P. Kulu, E. Talimets, and V. Mikli, *Surf. Coat. Technol*. **114**, 129 (1999).
10. V. K. William Grips, H. C. Barshilia, V. E. Selvi, and K. S.

Rajam, *Thin Solid Films*, **514**, 204 (2006).
11. B. Wu, Y. Fu, J. Xu, G. Lin, and M. Hou, *J. Power Sources* **194**, 976 (2009).
12. H. Wang, M. P. Brady, G. Teeter, and J. A. Turner, *J. Power Sources* **138**, 86 (2004).
13. Y. Wang and D. O. Northwood, *J. Power Sources* **165**, 293 (2007).
14. H. Wang, M. A. Sweikart, and J. A. Turner, *J. Power Sources* **115**, 243 (2003).
15. Y. Wang and D. O. Northwood, *J. Power Sources* **191**, 483 (2009).
16. H. Wang and J. A. Turner, *J. Power Sources* **128**, 193 (2004).
17. I. H. Oh and Jae-Bong Lee, *Corros. Sci. Tech*, **9**, 129 (2010).
18. A. Pozio, R. Silva, F. M. De Francesco, and L. Giorgi, *Electrochim. Acta.* **48**, 1543 (2003).